Soft Matter

PAPER

View Article Online
View Journal

Cite this: DOI: 10.1039/d5sm00748h

Emulsification of lyotropic lamellar phases: new formulation routes for stabilized water-in-water emulsions

Yohann Chapuis,[a] Daniel Ackermann,[a] Florian Martinez,[a] Zoé Lecomte,[a] Andréa Dibamba,[a] Louise Labeyrie,[a] Noëmie Coudon,[a] Ahmed Bentaleb,[a] Jean-Paul Douliez,[b] Etienne Ducrot,[a] Nicolas Martin,[a] Frédéric Nallet *[a] and Laurence Navailles*[a]

Stabilizing water-in-water emulsions remains a key challenge in soft matter science, with growing relevance for applications such as microencapsulation in food technology, bioseparation, and the construction of synthetic cells. Building on recent advances in interfacial self-assembly of fatty acid bilayers, we present here a robust and tunable strategy for stabilizing polyethylene glycol/dextran aqueous two-phase system emulsions using lyotropic lamellar phases doped with phase-separating polymers. We show that these lamellar phases spontaneously adsorb at the droplet interface, forming a stabilizing interfacial coating. By comparing multiple formulation routes, including lamellar phase pre-assembly with or without excess solvent and the previously used "one-pot" method, we demonstrate that all approaches yield equivalent droplet stabilization. Systematic variation of the lamellar phase concentration reveals a critical threshold necessary for emulsion stability. Beyond this threshold, excess lamellar material is dispersed into the continuous phase. A simple geometric model supports the hypothesis that this critical concentration corresponds to the amount required to fully coat the droplet interfaces. This strategy offers a straightforward yet precise formulation route that leverages the self-assembly and dilution behavior of lamellar phases, opening new avenues for designing fully aqueous emulsions stabilized without solid particles or synthetic surfactants.

Received 22nd July 2025,
Accepted 23rd September 2025

DOI: 10.1039/d5sm00748h

rsc.li/soft-matter-journal

1 Introduction

Aqueous two-phase systems (ATPS), or water-in-water (W/W) emulsions, result from the phase separation of hydrophilic solutes such as polymers, salts, ionic liquids, or biomacromolecules into two immiscible aqueous phases.[1] As they do not require oil or organic solvents and can spontaneously partition biomolecules, W/W emulsions have attracted increasing interest in applications such as bioseparation, food science, and synthetic cell design.[2–4] Like conventional oil–water emulsions, W/W systems are thermodynamically unstable, prone to coarsening and eventual macroscopic demixing. Expanding their functional scope therefore requires effective stabilization strategies. However, the interfacial properties of W/W emulsions differ fundamentally from those of oil–water systems, which challenges traditional stabilization approaches. Their ultralow interfacial tensions[5] (typically 0.001–0.1 mN m^{-1}) and extended interfacial thicknesses (up to one micrometer[6]) render many conventional surfactants monolayers ineffective. While various strategies have been explored to stabilize ATPS, notably using polymers,[7–9] proteins,[10–12] or soft particles like microgels[13,14] or liposomes,[15] general and predictive stabilization mechanisms remain elusive.

One promising direction takes inspiration from microemulsions, which are thermodynamically stable dispersions where surfactant molecules self-assemble into interfacial structures. Among these, lyotropic lamellar phases, composed of periodically stacked bilayers separated by water layers,[16] offer a particularly appealing example. Their structural properties, such as periodicity, bending rigidity, and permeability, can be finely tuned *via* composition or doping.[17] In particular, the lamellar periodicity can be adjusted across a broad range by varying solvent content: from a few nm in minimally hydrated systems to several hundred nm in highly swollen ones. This swelling behavior was first interpreted theoretically in terms of an effective repulsive interaction between bilayers,[18] known as "undulation", and later refined by invoking an unbinding transition,[19,20] which was

[a] Univ. Bordeaux, CNRS, CRPP, UMR 5031, F-33600 Pessac, France. E-mail: laurence.navailles@crpp.cnrs.fr
[b] Univ. Bordeaux, INRAE, Biologie du Fruit et Pathologie, UMR 1332, 71 Avenue Edouard Bourlaux, 33140 Villenave d'Ornon, France

validated experimentally.[21,22] More specifically, depending on hydration, two distinct regimes emerge. In the "swelling" regime (low solvent content), bilayers incorporate all available solvent between them, and the lamellar period increases linearly with hydration. Beyond a critical threshold (known as the dilution or swelling limit), further solvent no longer enters the stack, leading to a "bound" regime where a lamellar phase with fixed periodicity coexists with excess solvent. In rare cases, unbound regimes are observed, where lamellar phase continue to swell indefinitely, with periodicity diverging as hydration increases.

The polymorphism of doped-solvent or doped-bilayer lamellar phases has attracted considerable interest over more than 4 decades, with pioneering and recent contributions.[23–28] Doping lamellar phases with polymers or particles adds further versatility, making them attractive candidates for stabilizing complex aqueous interfaces.[29,30] In a recent work, we showed that W/W emulsions could be effectively stabilized by a multilamellar interfacial coating.[31] The formulation route simply relied on the addition of sodium oleate and 1-decanol to a suspension of dextran (DEX)-in-polyethylene glycol (PEG) droplets under vigorous shaking to nearly instantaneously produce uniformly-sized micro-droplets forming a kinetically-stable emulsion. At that pH of 9.9, the fatty acids are under the carboxylate (COO–) form and make hydrogen bonds with the hydroxyl group of decanol, allowing stabilization of the bilayer assembly (*vs.* micelles, for instance).[32] By combining freeze-fracture transmission electron microscopy and small-angle X-ray scattering (SAXS), we showed that the interfacial coating was composed of multiple lipid bilayers interspaced by large solvent layers, corresponding to a swollen lamellar phase.

Here, we extend this concept and present a general strategy for stabilizing W/W emulsions by emulsifying pre-formed lyotropic lamellar phases doped with phase-separating polymers (Fig. 1). We show that these phases spontaneously adsorb at the droplet interface, forming interfacial multilamellar shells that prevent coalescence. By comparing multiple formulation routes (Fig. 1), we demonstrate that our new emulsification strategy, with and without excess solvent, is strictly equivalent to the previously reported "one-pot" method. Importantly, SAXS reveals the formation of swollen lamellar phases with periodicities up to hundreds of nanometers in the dilution regime below the swelling limit. A simple geometric model supports our interpretation that the critical concentration corresponds to the amount required to coat all droplet surfaces. By varying the amount of lamellar phase in the emulsion, we further demonstrate, using confocal fluorescence microscopy, the existence of a critical minimum concentration of the lamellar phase necessary to achieve full interfacial coverage and stable emulsions. Beyond this threshold, excess lamellar material remains dispersed in the continuous phase.

Overall, this method leverages the well-characterized structure and phase behavior of lamellar systems to provide a robust and tunable stabilization strategy for W/W emulsions. By enabling precise interfacial engineering, our approach opens new routes toward designing fully aqueous emulsions with responsive or functional interfaces for applications in encapsulation, delivery, or artificial cell technologies.

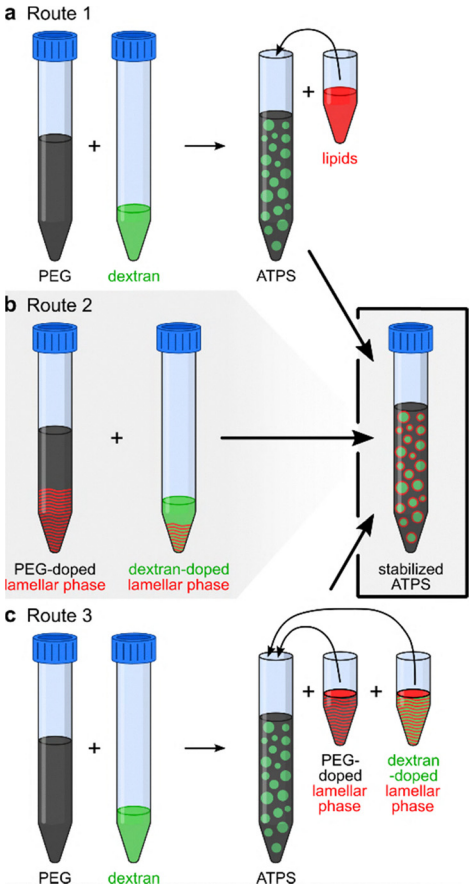

Fig. 1 Schematic representations of the three formulation routes for ATPS stabilized by lamellar phases. (a) Route 1: "one-pot" formulation method used in our previous work.[31] (b) Route 2: emulsification of two lamellar phases in excess solvent. (c) Route 3: emulsification of ATPS by lamellar phases at their limits of dilution.

2 Results and discussion

2.1 Structural properties of polymer-doped lamellar phases

To establish a reference for the structure and behavior of the lamellar phases in the different aqueous environments, we first characterized their properties in polymer solutions without any phase separation. This allowed us to identify distinct swelling regimes and probe interactions between the lamellar domains and surrounding polymers.

2.1.1 Optical characterization. Lamellar phases were formulated at various surfactant concentrations to span both the "swollen" and "bound" regimes. Building on our previous formulation, we used a fixed 1 : 3 molar ratio of sodium oleate to 1-decanol as the amphiphilic system. Two aqueous polymer stock solutions (PEG at 8.5 wt% and DEX at 13 wt%) were used to hydrate the lamellar phase. At these concentrations, PEG and DEX are in the dilute and semi-dilute regimes, respectively (Fig. 1S). Macroscopic observations of lamellar phases prepared at 3 different surfactant concentrations (20, 8 and 1 wt%) showed that all samples appeared homogeneous and weakly turbid, regardless of polymer identity (Fig. 2(a)). Yet, sample flow properties strongly depended on surfactant concentration,

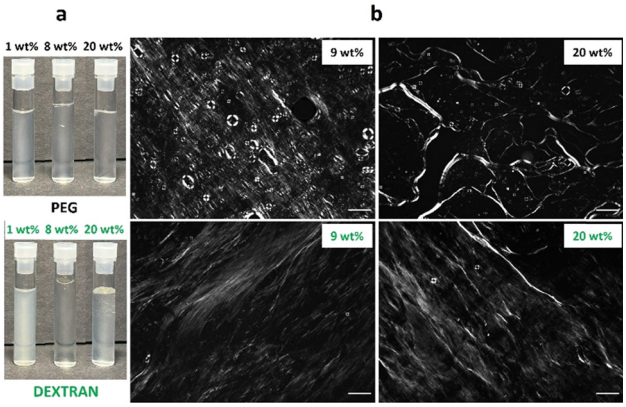

Fig. 2 Optical observation of lamellar phases as a function of surfactant concentration. (a) Macroscopic observation of samples hydrated with an aqueous solution at 8.5 wt% PEG (top) or 13 wt% DEX (bottom) at a surfactant concentration of 20, 8 and 1 wt%, as indicated (glass vials 8 × 40 mm, diameter × height). (b) Polarized light microscopy images of samples hydrated with 8.5 wt% PEG (top) or 13 wt% DEX (bottom) in the concentrated regime at 9 and 20 wt%, as indicated. Scale bars, 100 μm.

ranging from highly viscous, non-flowing samples (20 wt%) to free-flowing samples for the most dilute system (1 wt%).

Polarized light microscopy (Fig. 2(b)) confirmed the presence of birefringent textures characteristic of an optically anisotropic system. Defects such as oily streaks and spherulites typical of a lamellar phase were further observed.[33]

2.1.2 Structural characterization. To gain deeper insight into the structure of these polymer-doped lamellar phases, we conducted SAXS experiments on the entire dilution range. As an example, Fig. 3 shows the diffractograms in the swelling (Fig. 3(a): 10 and 5 wt% surfactant concentration) and bound (Fig. 3(b): 0.4 wt%) regime respectively, for both polymer-doped solvents.

In the swelling regime, diffractograms revealed a series of intense, narrow Bragg peaks indicative of a concentrated lamellar stack of bilayers (Fig. 3(a)). In addition, broader and weaker Bragg peaks were observed at slightly larger periodicities (lower q), also compatible with a one-dimensional, but more dilute, periodic stacking of bilayers. These two distinct families of peaks are consistent with lamellar–lamellar phase coexistence, a feature previously reported in lyotropic lamellar systems.[34–37] Upon dilution (from 10 to 5 wt% lipids), all Bragg peaks shifted to lower angles, reflecting an increase in lamellar spacing. The presence of multiple peak orders with 1 : 2 : 3 spacing ratios, when observed, confirmed the lamellar symmetry and supported the birefringent textures observed by polarized light microscopy (Fig. 2(b)).

In contrast, SAXS patterns obtained at much higher dilution (0.4 wt%, Fig. 3(b)) showed only a single, broad set of peaks with weaker intensity. The lamellar symmetry remained plausible

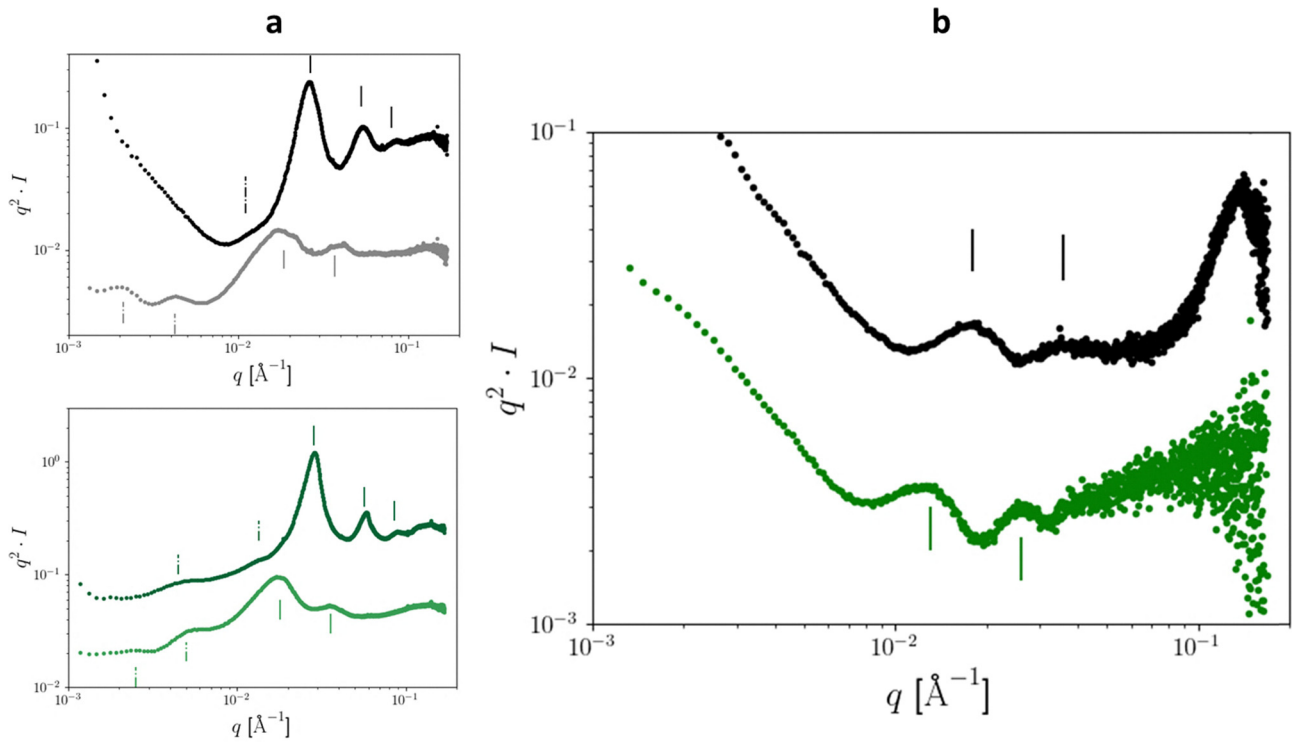

Fig. 3 SAXS of lamellar phases for selected surfactant concentrations in PEG (black) or dextran (green) aqueous solutions. Kratky representation of the scattered intensity (Iq^2 *vs.* q). The vertical lines indicate the position of different families of Bragg peaks and their harmonics (continuous line for the concentrated domain and dotted line for the diluted domain). (a) Diffractograms in the high concentration domain for two concentrations of surfactants at 10 (dark symbols) and 5 wt% (light symbols) hydrated by PEG (top) or dextran (bottom) solutions. (b) Diffractogram in the low concentration domain at a concentration of 0.39 wt% for PEG and 0.43 wt% for dextran aqueous solutions (green).

from the presence of the first and second orders, but the increased peak width indicated a much weaker correlation between the bilayers in this bound regime, where solvent no longer swells the phase, than in the more concentrated swelling regime. Interestingly, the (bound) lamellar periodicity depended on the polymer identity: approximately 35 nm for PEG-based samples and 50 nm for DEX-based samples. The difference in polymer conformation and entanglement status (Fig. 1S) may explain this difference in swelling limits due to a variation in the attractive/repulsive balance in interactions between bilayers. Overall, the results highlight the role of polymers in modulating the structural properties of lamellar phases.

To characterize how polymer-doped lamellar phases evolve with dilution, we systematically quantified the lamellar periodicity (d) as a function of the inverse of the surfactant volume fraction ($1/\varphi$) across the entire dilution range (Fig. 4). Swelling and bound regimes were actually identified from these measurements.

In the swelling regime (high surfactant concentration, low $1/\varphi$ values), periodicity increased approximately linearly with dilution, consistent with progressive insertion of polymer solution between bilayers without free excess solvent, in accordance with the so-called ''one-dimensional geometrical dilution law''—more details in Section S2. This regime spanned a wide concentration range for both polymer systems, and also applied to both lamellar structures observed in the SAXS patterns (Fig. 3(a)).[35–37]

Notably, the more dilute coexisting lamellar phase could swell significantly, with periodicities reaching up to 500 nm for the DEX-based samples.

At higher dilution ($1/\varphi > 40$ for DEX, >25 for PEG), variability in periodicity increased markedly, particularly for samples prepared with DEX. Measurements on different capillaries from the same batch showed variations of several tens of nanometers, and vertical scans along a single capillary confirmed this spatial heterogeneity (Fig. 2S). This poor repeatability, more pronounced in DEX-based systems, is likely due to the slow equilibration, in particular for entangled polymer chains above their overlap concentration c^* (Fig. 1S).

Despite this dispersion, a bound regime could be clearly identified for the more concentrated lamellar structure in each system. In this regime, periodicity reached a plateau, approximately 45 nm for PEG and 60 nm for DEX, indicating that the additional solvent was no longer incorporated between bilayers. These thresholds correspond to surfactant concentrations of $\sim$4 wt% for PEG ($1/\varphi \approx 25$) and $\sim$2.8 wt% for DEX ($1/\varphi \approx 35.7$). This behavior marks the transition from a swelling regime, where repulsive interactions dominate and inter-bilayer solvent increases, to a bound regime where repulsive and attractive interactions (*e.g.*, van der Waals and steric undulation interactions) balance. Interestingly, no bound regime was observed for the more dilute coexisting lamellar phase, even under optimized SAXS conditions on the SWING beamline. This phase apparently continues to swell indefinitely, suggesting that it remained unbound across the studied dilution range. These results highlight that the theoretical description of unbinding transitions for binary lamellar systems may need to be extended to three-component systems to account for the more complex, binary solvent conditions (polymer + water) investigated here.

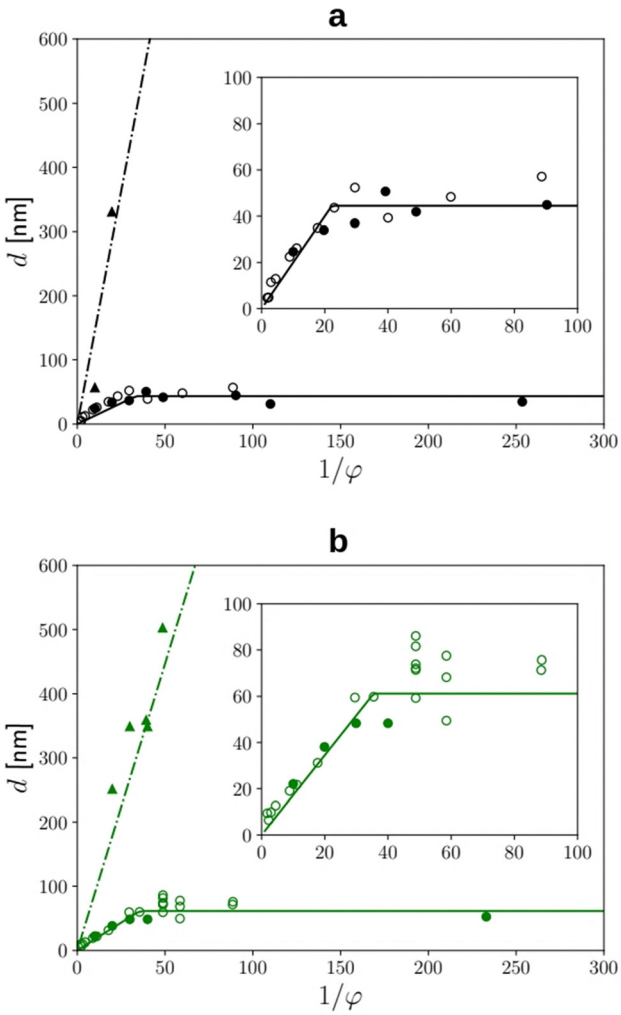

Fig. 4 Dilution laws of the coexisting lamellar phases as a function on the aqueous polymer solution content. Evolution of the lamellar periodicity (d) as a function of the inverse of the surfactant volume fraction ($1/\varphi$), (a) with PEG, and (b) with dextran. Solid or dash-dotted lines correspond to a non linear, least squares fit of a model—see details in the SI—to the lamellar periodicity data. Insets provide zoomed views of the high-concentration region. Filled and empty symbols show data obtained from synchrotron SWING beamline and laboratory XEUSS 2.0, respectively. For synchrotron data, triangles show results for the more dilute coexisting lamellar phase.

2.2 Emulsification of lamellar phases

Having established the structural behavior of polymer-doped lamellar phases across dilution regimes, we next explore their capacity to stabilize interfaces in PEG–DEX aqueous two-phase systems (ATPS).

To this end, the phase diagram of the PEG and DEX system was constructed experimentally (see Fig. 3S), and two distinct tie lines were selected to define the polymer compositions of the dispersed and continuous phases. These compositions were chosen to mimic direct (DEX-in-PEG) and inverse (PEG-in-DEX)

emulsions, corresponding to two points on the phase diagram connected by separate tie lines.

We previously explored a "one-pot" approach (route 1, Fig. 1(a)), where surfactants were added to a dispersed PEG/DEX polymer mixture followed by vigorous shaking to induce self-assembly at the droplet interface.[31] Here, we explored an alternative "post-assembly" strategy (route 2, Fig. 1(b)): lamellar phases were first pre-formed in excess solvent in the bound regime using either PEG or DEX solution, and then mixed together to match the chosen final polymer compositions in the ATPS phase diagram (direct or inverse emulsion).

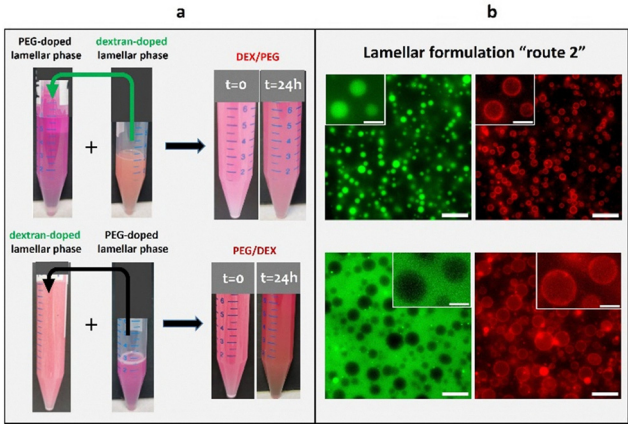

Fig. 5 Emulsification of lamellar phases in excess of solvent. Formulation of direct (top) DEX/PEG and inverse (bottom) PEG/DEX emulsions. (a) Macroscopic observation of doped lamellar phases and emulsions at t = 0 and 24 h after formulation. Lamellar phases were prepared at 0.4 wt% and 0.6 wt% surfactant for the direct and inverse emulsions, respectively. Nile red and FITC-dextran were added to stain surfactants-rich and dextran-rich regions, respectively. (b) Confocal fluorescence microscopy images of the stabilized emulsions with the fluorescence associated with dextran (green) and surfactants (red). Scale bars: 20 and 5 μm (zoomed images).

2.2.1 Optical characterization. Following 5 minutes of mechanical stirring, a turbid, macroscopically homogeneous dispersion was obtained for both systems (Fig. 5(a)). The emulsions remained stable at room temperature with no visible phase separation after 24 hours, mirroring our previous results using route 1.[31] Fluorescence staining using fluorescein isothiocyanate-labeled DEX (FITC-DEX) and the hydrophobic probe Nile red allowed to visualize DEX-rich and surfactant-rich regions, respectively, using confocal fluorescence microscopy (Fig. 5(b)). Images confirmed the formation of DEX-rich droplets in PEG in the direct system and PEG-rich droplets in DEX in the inverse system. In addition, surfactant material appeared to accumulate at the droplet interfaces. Specifically, a uniform continuous coating around each droplet was observed, indicative of interfacial surfactant assembly. The emulsions exhibited a relatively broad droplet size distribution, with mean diameters of ∼4.5 μm for direct DEX/PEG emulsions and ∼10 μm for inverse PEG/DEX systems. No signs of droplet coalescence were observed over a 24 h period, confirming the stabilizing role of the surfactant coatings.

To define the critical amount of lamellar phase required to stabilize W/W emulsions, we introduced a third formulation strategy (route 3, Fig. 1(c)). In this method, the ATPS was first prepared at its final composition, and then emulsified with the two lamellar phases, each formulated at their dilution limit in PEG or dextran (*i.e.*, without excess polymer solution), and added at 1 : 1 volume ratio. This ensured that all added surfactant material contributed directly to interfacial stabilization, allowing us to probe the onset of emulsion stability as a function of lamellar phase content. No signs of droplet coalescence were observed over a 48 h period, confirming the stabilizing role of the surfactant coatings (see Fig. 5S). Fig. 6(a) presents confocal fluorescence microscopy images of direct and inverse ATPS emulsions stabilized using increasing concentrations of lamellar phase. As expected, DEX-rich droplets (green fluorescence)

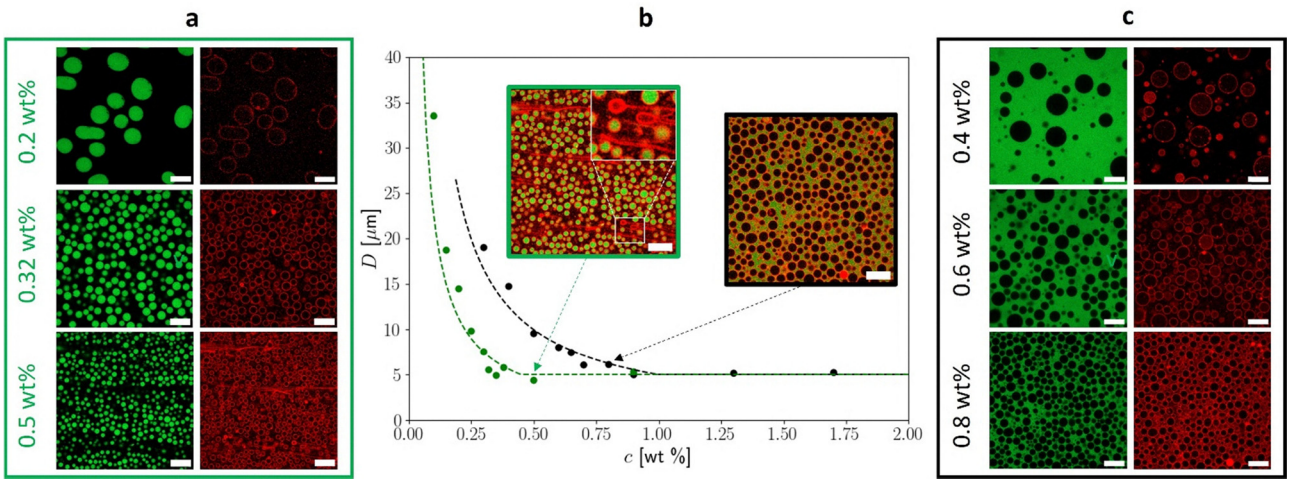

Fig. 6 Experimental determination of critical concentration in lamellar phase. (a) and (c) Confocal images showing the spatial distribution of FITC (green – dextran) and Nile red (red – lamellar phase) for different lamellar phase concentrations for the direct (a) and inverse (c) systems respectively. Scale bars, 20 μm. (b) Evolution of mean droplet diameter D as a function of lamellar lipidic concentration. Direct DEX/PEG system: green; inverse PEG/DEX system: black. The dotted line is an adjustment of the experimental points by the geometric model. The two images correspond to the superposition of the green and red channels at 0.5 wt% for the direct system (green box) and 0.8 wt% for the inverse system (black box).

dispersed in a continuous PEG-rich phase were produced in the direct system, while PEG-rich droplets (unlabeled) dispersed in a DEX-rich continuous phase formed in the inverse system. In both cases, surfactants (red fluorescence) were predominantly located at the droplets interface, indicating interfacial adsorption. However, at high surfactant concentration, excess lamellar material appeared in the continuous phase as non-droplet-associated red fluorescence, suggestive of multilamellar vesicles or aggregated lamellar stacks this was particularly visible in the PEG-rich phase of the direct system at 0.5 wt% surfactant (see zoom in the superposition of the green and red channels for the direct system).

More specifically, quantification of the evolution of droplet diameter with lamellar phase content revealed two distinct regimes across both systems (Fig. 6(b)). (i) At low lamellar phase concentrations, increasing the amount of surfactant led to smaller droplet sizes, consistent with progressive stabilization and coalescence suppression. As an example, in the direct system, droplet size decreased from ∼35 μm to ∼4.5 μm as surfactant content increases. (ii) Beyond a critical concentration, the droplet size plateaued. This regime marks the point where the system reaches saturation in interfacial coverage, consistent with excess surfactant material forming in the continuous phase.

2.2.2 Geometric model for emulsion stabilization. To rationalize the observed evolution in droplet size, we developed a simple geometric model based on physically grounded assumptions. For simplicity, droplet polydispersity was neglected. The model considers emulsification by route 3 at fixed stirring strength and time. Initially, small droplets form; however, if their interfaces are insufficiently coated by the lamellar phase, coalescence occurs.

This leads to larger droplets with reduced total interfacial area. The coalescence process continues until the amount of available lamellar phase is sufficient to fully and optimally coat the droplets surface, at which point droplet growth stops.

We further assume that, for a given ATPS composition, the water–water interfacial thickness is characterized by a length scale ξ, related to the distance to the critical point in the phase diagram. Optimal interfacial coverage is achieved when the number of stacked bilayers, n, satisfies the condition: $n \times d = \xi$, where d is the lamellar periodicity in the bound regime. Fig. 7 schematically illustrates the underlying geometrical criterion.

Assuming that the droplets diameter, D, is much larger than ξ, the number of surfactant molecules required to achieve optimal coating of a single droplet of area $A = \pi D^2$ is given by:

$$N = \frac{2nA}{\Sigma}$$

where Σ is the molecular area per surfactant at the bilayer/solvent interface. The factor 2 accounts for the two leaflets in each bilayer.

For an emulsion of total volume V, with a dispersed phase volume fraction ϕ_d (determined *via* the lever rule for a given ATPS composition), the total number of coated droplets (assuming equal size) is $\frac{6\phi_d V}{\pi D^3}$. Multiplying by the number of surfactants per droplet gives the total number of surfactant molecules needed for optimal coverage of all droplets:

$$N_{tot} = 12\frac{\xi\phi_d}{d\Sigma D}V$$

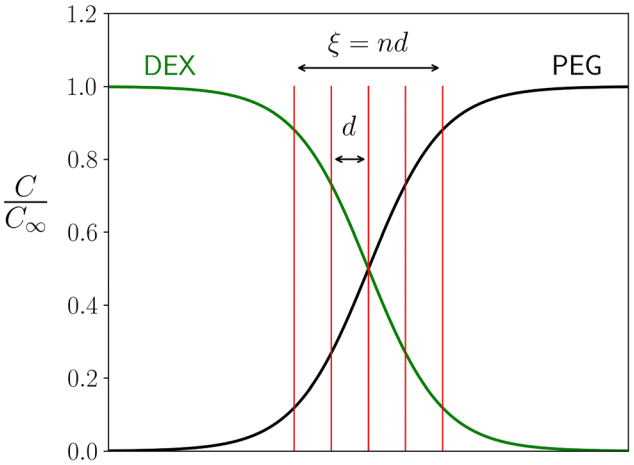

Fig. 7 Reduced polymer concentration profiles along a local axis normal to the dextran-rich/PEG-rich interface (left vertical axis). Planar projection perpendicular to the interface, with equally-spaced red lines representing lipid bilayers (right vertical axis, unlabeled). Spatial scale in terms of interfacial width ξ, chosen such that the appropriate polymer concentration has decreased by *ca.* 12% at the left-most/right-most lipid bilayer.

This expression reveals that the droplet diameter D is inversely proportional to surfactant concentration, assuming coalescence proceeds until optimal coverage is reached. Importantly, for a given emulsification energy, there exists a minimum achievable droplet size D_0 set by the initial fragmentation process. Therefore, surfactants added in excess of the threshold amount $12\frac{\xi\phi_d}{d\Sigma D_0}V$ cannot contribute to further droplet stabilization and are instead expected to self-assemble into multilamellar aggregates or vesicles, consistent with the excess of the red fluorescence observed in Fig. 6(a) at higher lamellar concentrations.

The dashed lines in Fig. 6(b) correspond to fits of this model to the experimental data. The parameters ξ (interfacial thickness) and D_0 (minimum droplet size) were treated as free-fitting variables, while d (stacking period) and ϕ_d (dispersed volume fraction) were fixed to experimental values (see Table 1). The surfactant molecular area was estimated from literature as $\Sigma \approx 0.27$ nm^2.[38] Given the clear experimental definition of D_0 (±0.6 μm), the fits provided an indirect estimate of the

Table 1 Model parameters values: volume fraction of the dispersed phase (ϕ_d), lamellar periodicity (d) at the dilution limit, interface thickness (ξ) and minimum droplet diameter (D_0)

	DEX/PEG	PEG/DEX
ϕ_d	0.18	0.32
d [nm]	45	60
ξ [μm]	0.39	0.65
D_0 [μm]	5	5

W/W interfacial thickness, ξ (with a relative error of about 30%, from standard error propagation formulae), reported in Table 1.

2.2.3 Structural characterization. While microscopy provided evidence for interfacial stabilization by lamellar assemblies, we turned to SAXS to directly probe the internal structure of the surfactant layers at the interface and assess their resemblance to the bound lamellar phases characterized earlier.

Given the low surfactant concentrations in the dispersions, samples were centrifuged to promote phase separation and enrich the lamellar phase content at the interface, thereby enhancing scattering contrast (see methods for details).

After centrifugation, three distinct zones were observed: a clear transparent upper phase, a slightly greenish transparent lower phase, and a turbid, somehow pink interfacial region (inset Fig. 4S).

SAXS experiments confirmed the known scattering behavior of the polymer solutions (Fig. 4S) the supernatant PEG-rich phase (upper part of the capillary in Fig. 4S) exhibited a scattering intensity decay with a $1/q^2$ law, consistent with a polymer in a theta solvent, whereas the dextran-rich sub-phase (bottom part of the capillary colored in green in Fig. 4S) followed a $1/q^{5/3}$ dependence, indicative of a polymer in good solvent conditions. Fluorescence microscopy further corroborated this separation, with the upper PEG-rich phase appearing dark in both green and red fluorescence channels, and the lower phase showing a uniform green fluorescence signal consistent with dextran predominance.

The part at the interface between the two polymer solutions, which appears pink (software enhanced red color) on the capillary in Fig. 4S, is the lamellar phase. To evaluate the impact of formulation on the lamellar phase structure, we compared the three emulsification routes shown in Fig. 1. Fig. 8 presents SAXS data (in Kratky representation) for both the direct (light red) and inverse (dark red) systems. In all cases, the scattering curves exhibit two Bragg peaks that could be indexed by q_0 and $2q_0$, a signature of lamellar symmetry. While the peak positions remain unchanged across different formulation routes for a given composition, a clear difference in periodicity emerges between the two systems, with a first order peak q_0 around 0.017 $Å^{-1}$ and 0.012 $Å^{-1}$ for direct DEX/PEG and inverse PEG/DEX systems, respectively. To further interpret these findings, Fig. 9 compares the SAXS patterns from emulsified systems to those obtained for separate lamellar phases prepared at their dilution limit in either PEG (black curve) or dextran (green curve) solutions.

Despite the low scattering intensity and broad peaks, attributable to the small amount of organized material, the results clearly show that in the direct system, the signal closely matches that of a lamellar phase hydrated with PEG solution (at 4 wt% surfactant), while in the inverse system, the signal resembles that of a lamellar phase hydrated with dextran solution (at 2.8 wt% surfactant). A weak contribution from a dextran-doped bound lamellar phase is nevertheless visible in the direct system formulated *via* route 3 in Fig. 9, where dextran forms the dispersed phase. However, given that nothing favors from a thermodynamic point of view the coating of W/W emulsion interfaces by either PEG- or dextran-doped bound lamellar phases, we cannot propose a definitive explanation for these possibly fortuitous observations.

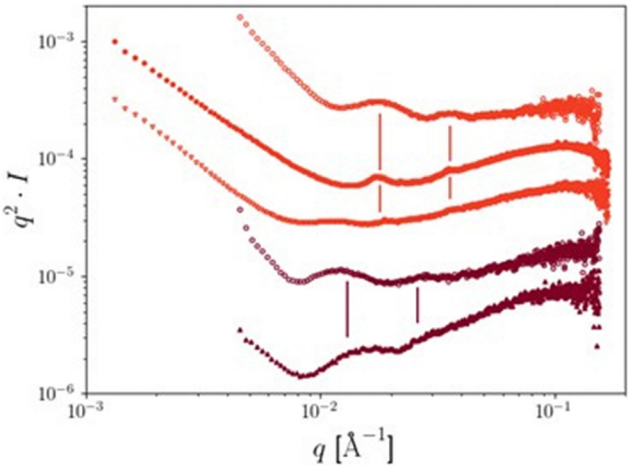

Fig. 8 Structural characterization of emulsions stabilized by lamellar phases using three different formulation routes. Scattered intensity in the Kratky representation as a function of wave vector q for the direct system (light red curves) and for the inverse system (dark red curves). For convenience and better readability, data has been vertically shifted by appropriate factors. The three formulation routes are represented by three different symbols: empty circles for route 1, solid circles for route 2 and triangles for route 3. The vertical lines indicate the position of the Bragg peaks of first (q_0) and second ($2q_0$) order.

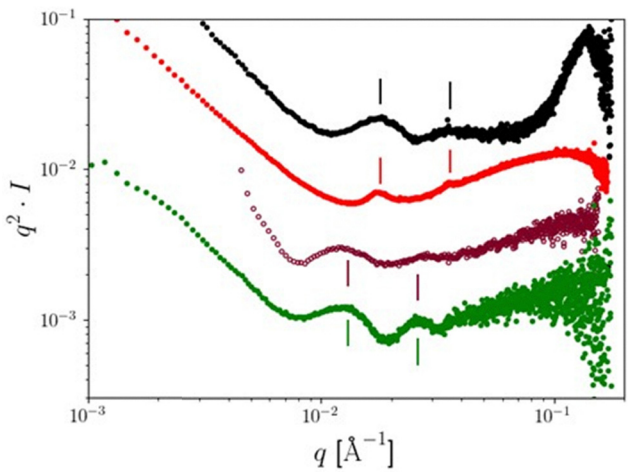

Fig. 9 Structural characterization of emulsions stabilized by lamellar phases at their dilution limits. Scattered intensity (Kratky representation) as a function of the wave vector q for the two stabilized direct (light red curve) and inverse (dark red curve) emulsions as well as for the two lamellar phases at the dilution limit hydrated with either the PEG solution (black curve), or the dextran solution (green curve). For convenience and better readability, data has been vertically shifted by appropriate factors. The vertical lines indicate the position of the Bragg peaks of first (q_0) and second ($2q_0$) order.

3 Conclusions

We have presented here a new method for stabilizing ATPS by emulsifying lyotropic lamellar phases. By systematically studying

the dilution behavior of lamellar phases formed from sodium oleate and 1-decanol in PEG and dextran solutions, we identified distinct dilution limits for each system. Beyond these limits, the lamellar phase enters a "bound" regime, where additional solvent remains in excess. Considering lipid concentration, both bound regimes are rather dilute, the lamellar periodicity reaching approximately 45 nm in PEG solution (at 8.5 wt%) and around 60 nm in dextran solution (at 13 wt%). In the swelling regimes, that is to say at higher lipid concentrations, a biphasic lamellar region appears, characterized by the coexistence of two lamellar phases, one swelling to periodicities as high as 500 nm in dextran solution, and the other reaching its polymer-dependent dilution limit $\sim$50 nm.

Based on this structural understanding, we developed two new formulation routes for preparing emulsions: direct emulsification of lamellar phases dispersed in excess solvent, and the addition of lamellar phase at defined concentrations to preformed ATPS. In both cases, stable emulsions were obtained. Crucially, these approaches enabled us to define a critical concentration of lamellar phase required for stabilization, which we hypothesize corresponds to the amount needed to fully coat the droplet interfaces. This hypothesis is supported by a simple geometric model describing the relationship between droplet size and surfactant content that leads to reasonable estimates for the interfacial thickness in two systems.

Our findings point to a simple and versatile method for stabilizing water-in-water emulsions: simple, because it involves direct mixing of lamellar phases with the ATPS; and versatile, because the wide range of possible lamellar phase formulations opens avenues for tuning compartmentalization and encapsulation properties. Lamellar systems have long been studied for their structural polymorphism and their capacity to host guest species, such as polymers, polyelectrolytes, inorganic nanoparticles (*e.g.*, silica, magnetic particles, clay), and biomacromolecules (DNA, RNA, proteins, enzymes). These components can localize in different regions of the lamellar structure: within the bilayers, suspended in the aqueous phase, or adsorbed at the membrane interfaces. Beyond encapsulation, the permeability of lamellar bilayers can be modulated by external stimuli such as pH[39] or temperature,[40] allowing controlled release of active substances. Our approach offers new possibilities for designing ATPS emulsions with spatially and temporally controllable release, by exploiting stimulus-responsive lamellar membranes.

4 Materials and method

4.1 Materials

The following chemicals were purchased from Sigma-Aldrich and used as received: dextran (500 kg mol^{-1}; DEX), polyethylene glycol (20 kg mol^{-1}; PEG), sodium oleate, 1-decanol, Nile red, rhodamine isothiocyanate (RITC), fluorescein isothiocyanate-dextran (500 kg mol^{-1}, FITC-dextran), dimethylsulfoxide (DMSO) and ethanol. Milli-Q-purified water was used for all experiments.

4.1.1 Formulation of lamellar phases. The polymer stock solutions prepared to swell the lamellar phases were set as follows. The PEG stock solution has a weight concentration of 8.5%. For a total volume of *ca.* 20 mL, 1700 mg of PEG were weighed into 18.3 mL of Milli-Q water. The DEX stock solution has a weight concentration of 13%. For a total volume of *ca.* 20 mL, 2600 mg of dextran were weighed into 17.4 mL of Milli-Q water. The two stock solutions were prepared in glass containers and mixed under magnetic stirring for 24 h at room temperature to ensure complete polymer dissolution. These stock solutions were stored at 4 °C. To formulate the ATPS used in the formulation path with lamellar phases at the dilution limit (route 3) two other stock solutions at 12 wt% PEG and 16 wt% dextran were also prepared following the same protocol.

The lamellar phases were formulated as follows. In a 1.5 mL Eppendorf tube or 15 mL Falcon tube, we prepared lamellar phases of sodium oleate + decanol and PEG or dextran stock solution at the desired swelling state by weighing each component. The polymer solution in an appropriate amount for reaching the desired hydration of the lamellar phase was added last. To achieve thermodynamic equilibrium, samples were centrifuged (4 minutes at 2500 rpm) forwards and backwards four times a day and left radially on a rotating wheel (diameter *ca.* 195 mm, 14 rpm) for the rest of the day. This step was repeated for 7 days in order to reach homogeneity, checked visually. A 1 mM Nile red stock solution was prepared by dissolving an appropriate amount of solid dye in DMSO, and then a volume of 50 μL of this dye solution for 10 mg of lipids in the lamellar phase was added. A 2 wt% stock solution of FITC-dextran was prepared by dissolving a given amount of the polymer in Milli-Q water. The lamellar phase hydrated with dextran solution was fluorescently labeled by adding 40 μL of FITC-dextran stock solution to 5 mL of dextran solution to obtain a molar ratio between dextran and FITC-dextran equal to 230. In this way, we formulated different samples by varying the [decanol/sodium oleate]/polymer aqueous solution ratio to describe the complete dilution range from highly concentrated systems (approx. 60 wt% amphiphilic molecules) to extremely dilute systems (with around 1 wt% amphiphilic molecules). The two lamellar phases formulated with an excess of solvent (route 2) were prepared at a lipid concentration of 0.38 wt% in order to achieve the lipid concentration equivalent to the system formulated by the "one-pot" formulation route (route 1) of ref. 29. For the emulsification of ATPS by lamellar phases at their limits of dilution (route 3), the lamellar phase at the dilution limit for the PEG polymer solution was prepared at a lipid concentration of 4 wt%, while the dilution limit with the dextran polymer solution was at 2.8 wt%.

4.1.2 Preparation of aqueous multi-phase system (AMPS). Two compositions of ATPS were studied and formulated from stock solutions. We chose compositions on two different tie lines on the phase diagram to produce either DEX droplets in a continuous PEG phase (direct emulsion) or PEG droplets in a continuous DEX phase (inverse emulsion). To build the phase diagram (shown in Fig. 2S), the binodal line was constructed experimentally by observing the transition between a transparent and turbid sample by varying the PEG and DEX composition. The two tie lines were deduced experimentally from the binodal line by measuring the volume fractions of the dispersed and continuous phases for samples of known PEG and dextran concentrations.

Three formulation paths were then used to prepare stabilized emulsions (illustrated in Fig. 1). The "one-pot" formulation route (route 1) was described previously (ref. 29) and simply consisted of adding surfactants by pipetting to a vigorously stirred ATPS. To emulsify the two lamellar phases in the excess of solvent (route 2), the system with the lower volume was added to the system with the higher volume, and the mixture, in a glass bottle or in a Falcon tube, was stirred manually for 5 minutes. The total sample volume was 10 mL. For the AMPS formulation (route 3), the first step was to form the ATPS by mixing the appropriate volumes of the two polymer stock solutions during 3 minutes. In a second step, required volumes of lamellar phases at the dilution limit (and in a 1 : 1 ratio between the two lamellar phases hydrated with PEG and DEX solvent) were added to achieve the desired final lipid concentration in the emulsion. The sample was then stirred during 30 seconds.

4.2 Methods

4.2.1 Macro- and microscopic observations. Polarized light microscopy was performed on an Olympus BX 51 microscope with crossed polarizers using a moderate magnification (20× air objective). Samples were sandwiched between a glass slide (1 mm thick) and a coverslip (0.14 to 0.17 mm thick), with water evaporation prevented by a rim of a UV-cured glue. Confocal fluorescence microscopy was performed on a ZEISS LSM 980 Airyscan 2 microscope equipped with a 20× air or 63× oil immersion objective. Images were processed using Fiji software.[41] Chambers with a constant thickness or with a thickness gradient were created according to the sample under study. Dyes were excited by using the following excitation (λ_{ex}) and emission wavelengths (λ_{em}): FITC-dextran, λ_{ex} = 488 nm, λ_{em} = 495–565 nm; Nile red, λ_{ex} = 561 nm, λ_{em} = 630–760 nm.

4.2.2 Small angle X-ray scattering (SAXS). X-ray diffraction experiments were done on a XEUSS 2.0 device (XENOCS, Grenoble, France) with a GeniX3D system (XENOCS, microfocus copper anode source coupled to a FOX3D single reflection mirror) delivering a monochromatic 8 keV beam (CuKα radiation, wavelength λ = 1.5418 Å). The beam was further collimated by a set of two motorized scatterless (four-blade) slits. Exposure times depended on the concentration of surfactant in the samples. They were of the order of one hour for concentrated lamellar phases and 4 hours for diluted lamellar phases or stabilized ATPS. Data (487 × 619 pixels, pixel size 172 × 172 μm^2) were collected by a two-dimensional DECTRIS PILATUS-300k detector (Baden-Dättwill, Switzerland) placed at a sample-to-detector distance of around 2.50 m (calibrated with a silver behenate standard), that gives nominally access to scattering wave vectors q from $q = 8 \times 10^{-3}$ Å^{-1} to $q = 1.6 \times 10^{-1}$ Å^{-1} with a direct beam located horizontally close to 220 pixels from the left edge of the image, and vertically at 510 pixels from the top edge. The 1D diffractograms (intensity I *vs.* q) were obtained by processing the detector images with the FOXTROT software, developed jointly by XENOCS and SOLEIL synchrotron (Saint-Aubin, France). Some X-ray scattering patterns were also recorded at the SWING beamline of the SOLEIL synchrotron. A range of wave vector magnitudes of $q = 1 \times 10^{-3}$ Å^{-1} to $q = 1.78 \times 10^{-1}$ Å^{-1} was obtained with a photon energy of 12 keV by making experiments at a sample-to-detector distance of 6.21 m. The beam size was defined by a set of slits and was measured on the detector equal to 483 μm horizontally and 50 μm vertically. In all cases, *ca.* 20 μL sample volume was introduced into 1.5 mm optical path quartz glass capillaries (WJM-Glas Müller GmbH, Germany). The wall thickness was 0.01 mm. The capillaries were filled to a height of around 20 mm and sealed with a blowtorch at a height of 50 mm. They were then centrifuged (4000 rpm, 30 to 100 minutes) to induce phase separation between the lamellar and polymer-doped solvent phases. This step locally concentrates the lipids to increase the scattering signal (Bragg peaks) of the lamellar phase. The capillaries were then placed in a vertical position (to inhibit dispersion of the different phases) in static capillary holder with 15 to 20 positions. On the SWING beamline, the capillary holder was regulated at a temperature of 18.5 °C. An acquisition was always the sum of 5 images with counting times 1 s and gap time between each exposure of 0.5 s. Acquisitions were made either at a fixed position or along a vertical scan with 20 positions over an amplitude height of 3.2 mm within the scanning window. In this latter case and owing to hardware constraints, the vertical step was not exactly fixed, but always close to 0.16 mm. Data were collected by a two-dimensional DECTRIS EIGER 4M detector with 1083 × 1035 pixels in binning mode 2. Under these conditions, the size of each pixel was 0.15 × 0.15 mm^2. The center of the direct beam was located horizontally at 282 pixels from the left edge of the image, and vertically at 955 pixels from the top edge. FOXTROT was used for processing the detector images.

Author contributions

Yohann Chapuis: conceptualization, methodology, investigation, review and editing. Daniel Ackermann: conceptualization, methodology, investigation, review and editing. Florian Martinez: methodology, investigation, review and editing. Zoé Lecomte: methodology, investigation. Andréa Dibamba: methodology, investigation. Louise Labeyrie: methodology, investigation. Noëmie Coudon: methodology, investigation, review and editing. Ahmed Bentaleb: methodology, investigation. Jean-Paul Douliez: conceptualization, methodology, investigation, writing, review and editing. Nicolas Martin: conceptualization, methodology, investigation, supervision, writing, review and editing. Frédéric Nallet: conceptualization, methodology, investigation, supervision, writing original draft. Laurence Navailles: conceptualization, methodology, investigation, supervision, writing of the original draft, project administration.

Conflicts of interest

There are no conflicts to declare.

Data availability

Data supporting this article have been included as part of the Supplementary Information, including rheological characterisation

of PEG and DEX aqueous solutions, details about swelling and "bound" regimes – model and experiments, PEG/DEX/water experimental phase diagram, and details relative to stability of route 3 system. See DOI: https://doi.org/10.1039/d5sm00748h.

The raw small angle scattering data from beamline SWING is available to authenticated users in collection synchrotron-soleil-01, path /swing-users/20232065 of the GLOBUS system.

Acknowledgements

This work was funded by the French Agence Nationale de la Recherche (ANR-19-CE06-0013-02, ANR-24-CE06-7993). Laurence Navailles and Frédéric Nallet would like to thank Javier Perez and Thomas Bizien of the SWING beamline at the SOLEIL synchrotron for the rapid access to beamtime, proposal ID 20232065.

Notes and references

1 P. A. Albertsson, *Adv. Protein Chem.*, 2000, **24**, 309–341.
2 S. Daradmare and C. Lee, *Colloids Surf., B*, 2022, **219**, 112795.
3 A. Perro, N. Coudon, J. P. Chapel, N. Martin, L. Béven and J. P. Douliez, *J. Colloid Interface Sci.*, 2022, **613**, 681–696.
4 C. Xu, N. Martin, M. Li and S. Mann, *Nature*, 2022, **609**, 1029–1037.
5 L. Keal, C. E. Colosqui, R. H. Tromp and C. Monteux, *Phys. Rev. Lett.*, 2018, **120**, 208003.
6 E. Scholten, L. M. C. Sagis and E. van der Linden, *J. Phys. Chem. B*, 2004, **108**, 12164–12169.
7 D. M. A. Buzza, P. D. I. Fletcher, T. K. Georgiou and N. Ghasdian, *Langmuir*, 2013, **29**, 14804.
8 A. F. Mason, B. C. Buddingh', D. S. Williams and J. C. M. Van Hest, *J. Am. Chem. Soc.*, 2017, **139**(48), 17309.
9 Y. Ji, Y. Lin and Y. Qiao, *J. Am. Chem. Soc.*, 2023, **145**, 12576.
10 M. Abbas, J. O. Law, S. N. Grellscheid, W. T. S. Huck and E. Spruijt, *Adv. Mater.*, 2022, **34**, 2202913.
11 B. T. Nguyen, T. Nicolai and L. Benyahia, *Langmuir*, 2013, **29**, 10658.
12 A. A. Dharani, T. Abeysinghe, E. J. Young, A. T. Rowland, L. C. Dunshee, S. Urandur, M. O. Sullivan, C. A. Kerfeld and C. D. Keating, *Small*, 2023, 2308390.
13 L. Waldmann, D. N. T. Nguyen, S. Arbault, T. Nicolai, L. Benyahia and V. Ravaine, *J. Colloid Interface Sci.*, 2024, **653**, 581–593.
14 D. N. T. Nguyen, L. Waldmann, V. Lapeyre, S. Arbault, V. Ravaine, T. Nicolai and L. Benyahia, *J. Colloid Interface Sci.*, 2023, **646**, 484–492.
15 D. C. Dewey, C. A. Strulson, D. N. Cacace, P. C. Bevilacqua and C. D. Keating, *Nat. Commun.*, 2014, **5**, 4670.
16 V. Luzzati, H. Mustacchi, A. Skoulios and F. Husson, *Acta Crystallogr.*, 1960, **13**, 660–667.
17 R. M. Servuss, W. Harbich and W. Helfrich, *Biochim. Biophys. Acta*, 1976, **436**, 900–903.
18 W. Helfrich, *Z. Naturforsch.*, 1978, **33a**, 305–315.
19 S. T. Milner and D. Roux, *J. Phys. I*, 1992, **2**, 1741–1754.
20 S. Komura and D. Andelman, *EPL*, 2003, **64**, 844–850.
21 K. Bougis, R. Leite Rubim, N. Ziane, J. Peyencet, A. Bentaleb, A. Février, C. L. P. Oliveira, E. Andreoli de Oliveira, L. Navailles and F. Nallet, *Eur. Phys. J. E: Soft Matter Biol. Phys.*, 2015, **38**, 78.
22 R. Leite Rubim, B. B. Gerbelli, K. Bougis, C. L. Pinto de Oliveira, L. Navailles, F. Nallet and E. Andreoli de Oliveira, *Eur. Phys. J. E: Soft Matter Biol. Phys.*, 2016, **39**, 3.
23 P. Kékicheff, B. Cabane and M. Rawiso, *J. Colloid Interface Sci.*, 1984, **102**, 51–70.
24 P. Fabre, C. Casagrande, M. Veyssié, V. Cabuil and R. Massart, *Phys. Rev. Lett.*, 1990, **64**, 539–542.
25 M. Singh, R. Ober and M. Kleman, *J. Phys. Chem.*, 1993, **97**, 11108–11114.
26 E. Andreoli de Oliveira, E. R. Teixeira da Silva, A. Février, E. Grelet, F. Nallet and L. Navailles, *Europhys. Lett.*, 2010, **91**, 28001.
27 G. Castro Costa Leite and G. C. Castro Costa Leite, *J. Biol. Phys.*, 2021, **47**, 49–59.
28 A. Curkurent and O. Masalci, *Colloid Polym. Sci.*, 2025, **303**, 301–312.
29 M.-F. Ficheux, A.-M. Bellocq and F. Nallet, *Eur. Phys. J. E: Soft Matter Biol. Phys.*, 2001, **4**, 315–326.
30 V. Meklesh and P. Kékicheff, *J. Colloid Interface Sci.*, 2021, **582**, 1158–1178.
31 N. Coudon, L. Navailles, F. Nallet, I. Ly, A. Bentaleb, J. P. Chapel, L. Béven, J. P. Douliez and N. Martin, *J. Colloid Interface Sci.*, 2022, **617**, 257–266.
32 C. L. Apel, D. W. Deamer and M. N. Mautner, *Biochem. Biophys. Acta*, 2002, **1559**, 1–9.
33 I. Dierking, *Liq. Cryst.*, 2025, 1–33.
34 C. Ligoure, B. Bouglet and G. Porte, *Phys. Rev. Lett.*, 1993, **71**, 3600.
35 M. Singh, R. Ober and M. K1eman, *J. Phys. Chem.*, 1997, **97**, 11108.
36 G. Bouglet and C. Ligoure, *Eur. Phys. J. B*, 1999, **9**, 137–147.
37 M.-F. Ficheux, A.-M. Bellocq and F. Nallet, *J. Phys. II*, 1995, **5**, 823.
38 Y. Sasanuma, M. Nakamura and A. Abe, *J. Phys. Chem.*, 1993, **97**, 5155.
39 X. Zhanga, W. Zonga, H. Bib, K. Zhaoc, T. Fuhsa, Y. Huc, W. Chengd and X. Han, *Eur. J. Pharm. Biopharm.*, 2018, **127**, 177–182.
40 M. H. H. Tehrani, F. M. Kashkooli and M. Soltani, *Comput. Biol. Med.*, 2024, **170**, 108050.
41 J. Schindelin, J. Arganda-Carreras, E. Frise, V. Kaynig, M. Longair, T. Pietzsch, S. Preibisch, C. Rueden, S. Saalfeld, B. Schmid, J.-Y. Tinevez, D.-J. White, V. Hartenstein, K. Eliceiri, P. Tomancak and A. Cardona, *Nat. Methods*, 2012, **9**, 676–682.

